Coupling between Light and Terahertz-Frequency Acoustic Phonons in Ferroelectric $BaTiO_3/SrTiO_3$ Superlattices

A. Bruchhausen,[1,2] A. Fainstein,[1,*] S. Tinte,[3]
A. Soukiassian,[4] D. G. Schlom,[5] and X. X. Xi[1,5]

[1]*Centro Atómico Bariloche & Instituto Balseiro, CNEA, San Carlos de Bariloche, Río Negro, Argentina*
[2]*Department of Physics and Center for Applied Photonics, Unversity of Konstanz, Konztanz, Germany*
[3]*Instituto de Desarrollo Tecnológico para la Industria Química (INTEC), Santa Fe, Argentina*
[4]*Materials Research Institute, The Pennsylvania State University,University Park, PA, USA*
[5]*Department of Materials Science and Engineering, Cornell University, Ithaca, NY, USA*

(Received August 17, 2010)

The acoustic phonons in epitaxial ferroelectric $(BaTiO_3)_n/(SrTiO_3)_m$ superlattices (SLs) are investigated by high-resolution ultraviolet Raman scattering. The temperature dependence of the folded acoustic (FA) phonon Raman intensity through the ferroelectric transition is addressed. A comparison of this behavior between SLs with different number of ferroelectric $BaTiO_3$unit cells n and spacer $SrTiO_3$ unit cells m is presented. A mechanism involving the strain modulation of the spatially varying ferroelectric polarization is introduced to explain the temperature dependence of the FA phonon scattering. The temperature dependence of the polarization can be derived from an analysis of the first-order optical phonon spectra. Using this information, the observed temperature dependence of the whole set of SLs with different n can be consistently accounted for with the presented model. Atomistic shell-model simulations of the spatial pattern of the SL polarization are presented to explain the variation of the FA-spectral intensity for SLs with different m and the experimental fact that no high-order FA-replicas are observed. These results demonstrate the strong coupling between THz hypersound, charge, and light in these multifunctional nanoscale ferroelectrics.

PACS numbers: 78.30.-j, 78.20.hb, 77.90.+k

I. INTRODUCTION

Piezoelectric and ferroelectric materials are interesting in the search for stronger couplings between light and THz phonons and between the latter and charge [1–7]. This is particularly relevant for the development of more efficient THz phonon coherent sources and for the transduction of THz vibrations into THz electromagnetic radiation [8]. In this context, epitaxially grown ferroelectric oxide heterostructures and superlattices open an enormous field of research for the tailoring of multifunctional and complex properties that have been little studied so far. In fact, ferroelectric, piezoelectric, insulating, metallic, superconducting, and magnetic materials could be combined to provide a rich menu of physical properties and device performances.

Previous investigations of the ferroelectric properties of $(BaTiO_3)_n/(SrTiO_3)_m$ su-

perlattices have shown that reduced size, in combination with electrical and mechanical boundary conditions, can be exploited to tailor the physical properties of these nanoscale oxide ferroelectrics [9–14]. Materials that are usually not ferroelectric can become polarized, and the critical thickness of ferroelectric thin films can be reduced to a single unit cell. Their transition temperatures T_C can be tuned by hundreds of degrees in superlattices, their polarization can be enhanced, and their switching properties can be modified [9, 10, 15–17]. Oxide multilayers based on, for example, $BaTiO_3$ and $SrTiO_3$ can be also used to produce acoustic mirrors and cavities operative in the THz range with performance superior to similar semiconductor superlattices [18, 19].

On the basis of the investigations carried out at the end of the 1960's, we recently proposed that superlattices and herestructures made of these oxide materials could be particularly attractive in view of the expected strong coupling of the vibrational, charge, and light degrees of freedom [7]. These ferroelectric oxides become strongly piezoelectric below T_C. Additionally, evidence exists of a strong coupling in their bulk form between the acoustic vibrations and the polarization [20, 21]. On the other hand, the presence of a *permanent* polarization below T_C leads to a strong linear electro-optic coupling, which is proportional to the ferroelectric polarization [22]. These two specific features, namely a strong coupling between acoustic vibrations and polarization and between the latter and light are at the base of an additional and potentially strong elasto-optic coupling operative in the ferroelectric phase [22, 23]. The purpose of our investigation is to study how a spatial engineering of the ferroelectric polarization in nanostructured materials could be exploited to couple light with folded-acoustic high-frequency THz phonons using this mechanism.

In our previous letter we showed that the Raman intensity associated with folded acoustic phonons in $(BaTiO_3)_n/(SrTiO_3)_m$ superlattices (SLs) follows a temperature dependence that can be related to the onset of ferroelectricity in these materials [7]. We provide here a more detailed study that includes the complete set of spectra of the acoustic phonons in these man-made materials, and we also provide results on the dependence of the Raman-intensity on the thickness of the non-ferroelectric material $SrTiO_3$, i.e., on the number of unit cells m. We also provide a complete description of the applied phenomenological model that allows to better grasp the ingredients and assumptions involved. Our results indicate that a ferroelectric polarization-dependent elasto-optic mechanism that couples light with the folded acoustic phonons is operative in nanostructures where the polarization is spatially varying with the period of the SL. The specific ferroelectric polarization spatial pattern is thus relevant to describe the observed intensity of the observed folded-acoustic (FA) phonons. To address this issue we present atomistic shell-model simulations of these patterns and of their dependence with temperature. These calculations provide a framework to explain the observed temperature dependence of the FA phonon intensity and the non-observation of high-order replicas, and also to relate the observed Raman results to the formation of ferroelectric domains.

II. SAMPLES AND EXPERIMENTAL SET-UP

The $BaTiO_3/SrTiO_3$ SL samples were grown by reactive molecular-beam epitaxy [16, 24]. The substrate was (001) $SrTiO_3$ terminated at the TiO_2 layer, with BaO being the first layer deposited. The n and m values were controlled using reflection high-energy electron difraction (RHEED) oscillations during growth and confirmed by x-ray difraction (XRD) and in some samples by high-resolution transmission electron microscopy (HRTEM) [16]. XRD shows excellent epitaxy and crystallinity in the SL samples, with all SL peaks present in the θ-2θ scan. HRTEM images show atomically sharp $BaTiO_3/SrTiO_3$ interfaces and accurate periodicity [16]. According to XRD, all samples are commensurate to the $SrTiO_3$ substrate (a= 0.3905 nm), meaning that the $SrTiO_3$ layers are strain free and the $BaTiO_3$ layers are under 2.2% compressive biaxial strain (a= 0.3992 nm in bulk $BaTiO_3$ at room temperature),

Bulk crystalline $BaTiO_3$ (BTO) is cubic and paraelectric above T_C of 403 K, and it becomes tetragonal and ferroelectric below T_C. Unstrained bulk crystalline $SrTiO_3$ (STO) is paraelectric at all temperatures because of quantum fluctuations [14]. The devices studied here are epitaxially grown crystalline SLs. These are denoted by BTO_n/STO_m, where n and m refer to the thickness, in unit cells (u.c.), of the BTO and STO layers, respectively. The strain in the BTO layers induced by STO substrates leads to T_C larger than bulk [16]. Conversely, T_C is reduced when the number of atomic layers of BTO n is decreased as the dipole-dipole interaction between BTO layers becomes weaker. For this same reason thicker STO layers (m) suppress T_C by reducing the coupling between the polarized BTO layers [25]. The series of samples studied here were conceived to allow for the tuning of T_C essentially by changing n (n ranging from 1 to 8), while the degree of polarization of the STO layers was varied by controlling m (m being either 4 or 13). By these means, it is possible to tune T_C from 140 to 640 K [16].

Conventional visible Raman spectroscopy works poorly for thin films of ferroelectrics and other wide–band-gap materials because the visible photon energy is much smaller than the band gap [26]. Consequently, the absorption is extremely weak and the penetration depth is large, allowing light to travel through the film into the substrate, which generates overwhelming signals in the Raman spectra. For UV excitation, the photon energy is above the band gaps of ferroelectrics, leading to a much stronger absorption and a shorter penetration depth, preventing light from entering the substrate [16]. UV excitation near the band gap also leads to strong resonance enhancement of Raman signals. UV Raman spectroscopy has not been widely used for measurements of ferroelectric films because of technical difficulties such as lower throughput efficiency, insufficient dispersion, and higher stray-light level of UV Raman spectrometers as compared to those operating in the visible range. The recent progress in UV Raman instrumentation has made the measurement of ferroelectric films possible. To enable the present investigation, that aims to access the low-frequency folded acoustic vibrations, we have optimized the resolution and throughput of a triple monochromator Raman set-up to provide acoustic Raman spectra as close as 10 cm^{-1} to the UV 325-nm line of a HeCd laser, with a resolution better than 2 cm^{-1}. Spectra were recorded in both subtractive and additive configurations, in a back-scattering geometry

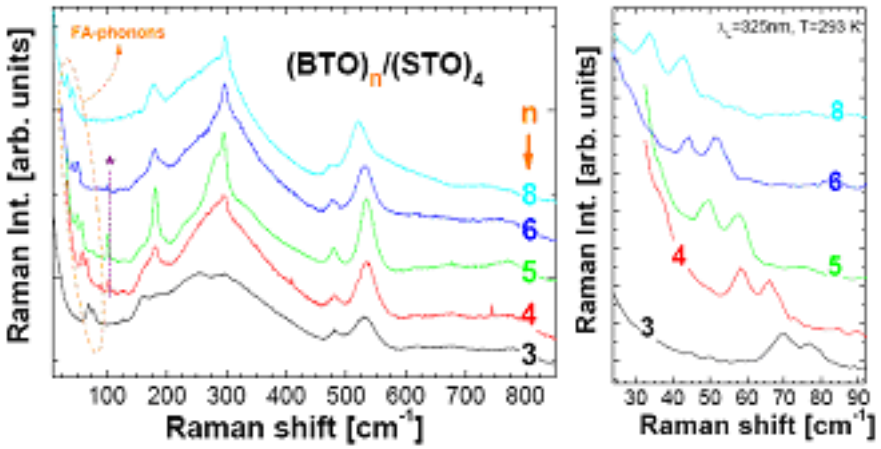

FIG. 1: Left: Typical UV-Raman spectra of BTO_n/STO_m superlattices with varying number of BTO unit cells n of 1 to 8 and m of 4. Strong first-order optic-phonon Raman peaks can be observed above $\sim$150cm^{-1}. Below 100cm^{-1}, the folded-acoustic (FA) Raman peaks appear that are displayed, in greater detail, in the right panel. Note that no higher-order FA phonon replicas are observed.

from 4 to 900 K using either a closed cycle cryostat (for low temperatures) or an evacuated heater stage (above 300 K). The laser power in all cases was around 10 mW, focused on an approximately 100-μm spot, controlled to avoid significant heating of the sample. Using this set-up, we have been able to observe low-frequency vibrational excitations to limits that have not been reported, to the best of our knowledge, so far.

III. EXPERIMENTAL RESULTS

Strong first-order (single-phonon) optical-phonon peaks can be observed below T_C in the UV-Raman spectra, as exemplified with the narrow lines observed above $\sim$150 cm^{-1}in the left panel of Fig. 1 for a series of BTO_n/STO_4 SLs of varying n. What is noteworthy in these spectra is the subject of this paper, i.e., the strong narrow doublets observed in the region between 30 and 80 cm^{-1} for the different samples, and this is shown in greater detail in the right panel of this same figure. These peaks are assigned to folded acoustic longitudinal (FA) phonons. Due to the SL periodicity, the acoustic phonon branches are folded back into the reduced Brillouin zone enabling their excitation by inelastic light scattering [27]. The spectral position of the doublets is determined by the size of the reduced Brillouin zone and thus by the SL period. We note that we have been able to observe, in all the studied samples, only the first zone-center FA doublets, and no high-order replicas. This contrasts with semiconductor SLs where several orders of phonon doublets are typically observed [5].

The presence of the first-order optic-phonons in the spectra of Fig. 1 can be taken as a

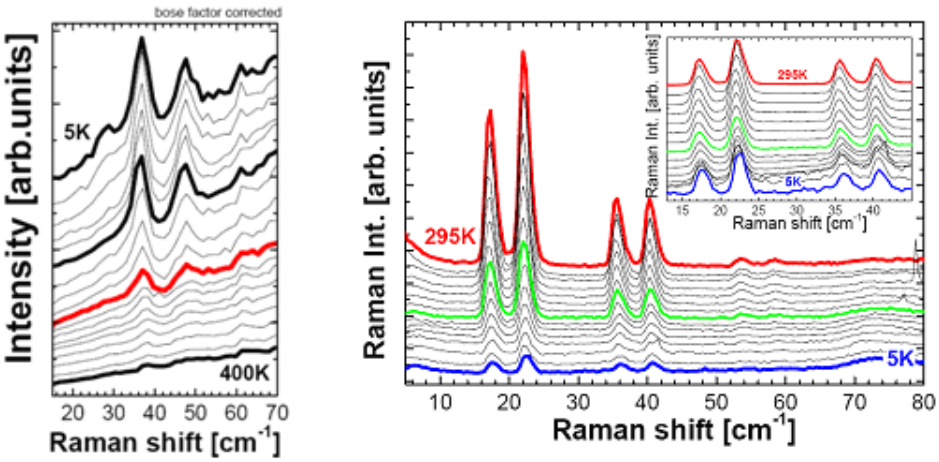

FIG. 2: Temperature variation of the Raman peaks corresponding to the FA doublet of a BTO_2/STO_{13} SL with T_C of approximately 200 K (left) compared with the behavior of a standard GaInAs/AlAs SL (right). The latter spectra were collected with visible 514.5nm excitation. The inset of the right panel displays the GaInAs/AlAs SL Bose-corrected FA spectra, which, as clearly observed, is independent of temperature.

signature of ferroelectric order and its disappearance with increasing temperature as a probe of the phase transition [16]. In fact, the observation of the optical first-order vibrations *only* below T_C follows from the lifting of the inversion symmetry that accompanies the phase transition to ferroelectric order. These modes are Raman forbidden in the paraelectric phase. What is completely unexpected and peculiar to these ferroelectric SLs is that the FA doublets also *decrease* their intensity with increasing temperature. This is illustrated for a BTO_2/STO_{13}SL with a transition temperature T_C of approximately 200 K in the left panel of Fig.2. In fact, in standard semiconductor SLs where this FA vibrations have been studied most [27], it is observed that the folded acoustic phonon intensity *increases* with increasing temperature following the phonon population given by the Bose factor (see the right panel of Fig.2).

We show in Fig.3 the temperature variation of the FA peak intensity for the studied superlattices with m of 13 and n ranging from 1 to 8 [7]. The spectra have been Bose corrected to discriminate standard effects due to the phonon population. Each curve is normalized to its respective T→0 value. The ferroelectric phase transition temperature T_C, derived from the behavior of the optic-phonon TO_4 peak, is shown for the different samples with dashed arrows. The FA peak intensity follows an onset-like behavior related to the appearance of the ferroelectric state. This is in sharp contrast with the discussed behavior of standard semiconductor SLs for which the FA-phonon intensity is essentially independent of temperature after Bose-correction is performed to the spectra (see right panel of Fig.2). Interestingly, as shown in Fig.3, the peak intensity does not remain constant once the ferroelectric order is established. In fact, it decreases when T approaches zero. This is particularly evident for the three samples with higher T_C. We note that the lifting

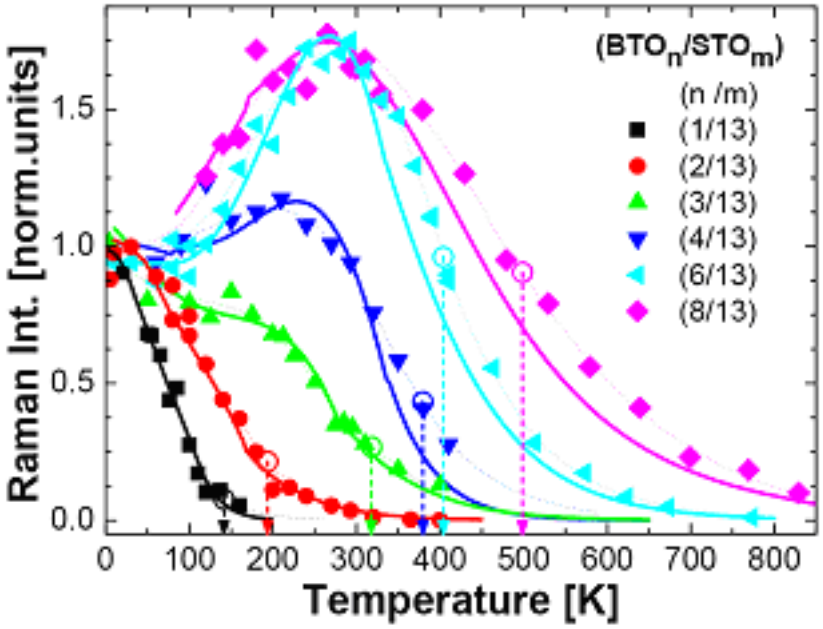

FIG. 3: Bose-corrected temperature dependence of the FA doublet intensity for a series of BTO_n/STO_m SLs with $m = 13$ and n ranging from 1 to 8. The measured values are normalized to the Raman intensity at T→0. The dashed arrows indicate the corresponding T_C derived from the temperature dependence of the TO_4optic-phonon peak intensity. The thin curves are guides to the eye. The thick curves correspond to the proposed ferroelectric polarization mediated scattering mechanism discussed in the text.

of inversion symmetry, as used to explain the observation of the first-order optical TO_4 mode *only* below T_C, cannot be invoked to explain the observed anomalous temperature behavior of the FA doublets.

As an additional property of the observed spectra we note that we have consistently observed that the FA-intensity is larger for superlattices with thicker STO layers (larger m). This is illustrated in Fig.4 for n of 3. The FA signals for m of 4 are only approximately 40% as intense as those observed in the sample with m of 13. From a comparison of the Raman signals of the SL series with m of 13 and m of 4, it also follows that FA peaks are observable for n of 1 and 2 (single and double unit-cell BTO layers) STO spacers with m of 13 *but not* for the thinner STO spacers with m of 4.

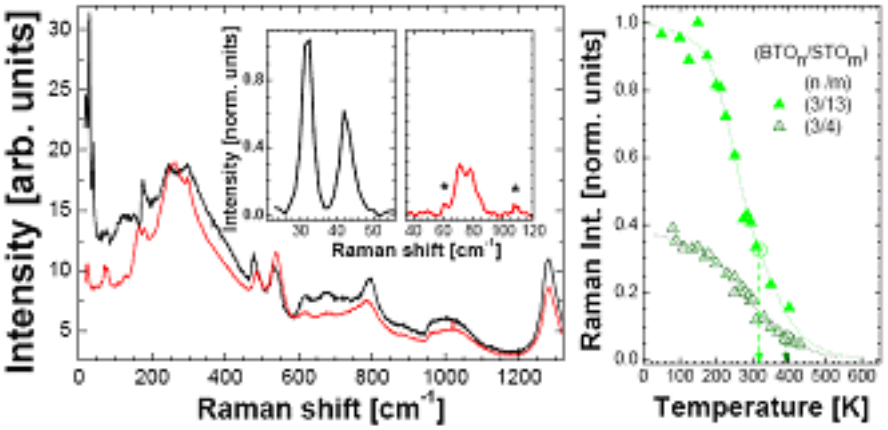

FIG. 4: Compared UV-Raman spectra for BTO_3/STO_m SLs with different STO spacers m of 4 and 13. (Left) Raman spectra taken at 200 K (red: m= 4, black: $m = 13$). Note the strong contrast in FA-intensity for the two samples (detail in inset). The asterisks indicate laser plasma lines. (Right) Temperature dependence of the FA-phonon intensity. Note that the transition temperature T_C is somewhat larger for m of 4 (as compared to the sample with thicker STO spacer m=14) due to the larger dipolar coupling between STO layers. The intensity of the FA-doublets for m of 4, on the other hand, is approximately 40% of that of the sample with m of 13 due to the smaller modulation of the ferroelectric polarization in the sample (see text for a detailed discussion).

IV. DISCUSSION

In what follows, we will present a model to account for the described temperature dependence of the FA-phonon Raman peaks in $BaTiO_3/SrTiO_3$SLs. The Raman scattering by acoustic phonons is given by [7, 27]:

$$\sigma(\omega) \propto \left[n(\omega+1)\right] \left| \int E_S^*(z) \Delta\chi(z) E_L(z) dz \right|^2 . \quad (1)$$

$\Delta\chi(z)$ is the change induced in the material dependent dielectric susceptibility by the acoustic phonon strain s, $\Delta\chi(z)(\partial\chi(z)/\partial s)\Delta s(z)$ ($s = \partial u(z)/\partial z$) with $u(z)$ the phonon displacement), and $E_L(E_S)$ is the laser(scattered) field. $n(\omega)$ corresponds to the statistical Bose-Einstein factor. In standard semiconductor SLs, the most important mechanism by which the strain modulates $\chi(z)$ is the deformation potential interaction. That is, the phonon strain modulates the electronic states, which in turn results in a time dependent variation $\Delta\chi$. The magnitude of this effect is usually expressed by the photoelastic constant $p(z) = \partial\chi(z)/\partial s$. The periodicity of $p(z)$ defines the accessible reciprocal lattice vectors and hence the possibility to observe FA vibrations. The intensity of the FA Raman scattered signal, on the other hand, is proportional to the *difference* of $p(z)$ between the two layers in the SL period. As $p(z)$ is only weakly dependent on the temperature through the

temperature variation of the optical gaps, the main effect of T is given by $n(\omega)$ in Eq. 1. Thus, FA intensities in semiconductor SLs are independent of temperature when the raw experimental data are Bose corrected, as experimentally verified with the data shown in the right panel of Fig.2. In contrast, for the oxide SLs studied here we have observed that the measured FA intensities *decrease* and disappear above T_C (see Figs.2 and 3). The electronic states determining the dielectric susceptibility are not significantly modified by the ferroelectric transition. Consequently, the standard photoelastic contribution should not change at T_C. Thus, an additional mechanism is required to explain our observations. The new mechanism should have the same periodicity of $p(z)$ (to account for the observation of standard FA doublets), should be absent above T_C (because the FA signal disappears in the paraelectric phase), and must be efficient so as to explain the observed strong FA Raman signals.

We propose that the inelastic scattering of FA phonons in these oxide SLs is mediated by the electric polarization P. The ferroelectric polarization in the BTO layers $P^{\rm BTO}$ develops below T_C, inducing a corresponding term in the paraelectric STO layers ($P^{\rm STO} \propto \chi_{\rm STO} P^{\rm BTO}$). Here $\chi_{\rm STO}$ is the dielectric susceptibility of STO. Thus, the ferroelectric polarization P in the BTO/STO SLs displays the same periodicity as the photoelastic constant $p(z)$. In addition to the standard photoelastic mechanism, the dielectric susceptibility in each material can be modulated by the phonon strain through $\Delta\chi(z) = (\partial\chi(z)/\partial P)(\partial P/\partial s)\Delta s(z)$. An effective photoelastic constant [23] thus adds to $p(z)$, which is given by $\pi(z) = (\partial\chi(z)/\partial P)(\partial P/\partial s)$. Here, $(\partial\chi(z)/\partial P)$ represents the electro-optic constant, which in the ferroelectric phase can be assumed to be linear with P through the quadratic electro-optic effect biased by the spontaneous polarization [22]. $(\partial P/\partial s)$ is the piezoelectric coupling, which is strong below T_C but becomes zero above T_C because of the centro-symmetric property of the cubic non-ferroelectric phase of the oxides. According to Eq.1, the Raman intensity by FA phonons should be proportional to the square of the *spatial modulation* of $\pi(z)$ (i.e., to the difference $\Delta\pi$ between the BTO and STO layers). As we show next, all the experimental observations can be consistently accounted for within this model.

We have calculated the Raman intensity using Eq. 1, with $\Delta\pi(z)$ given by the proposed P-mediated mechanism. An illustration of the applied procedure is presented in Fig.5. We first use the fact that $\pi(z) \propto P$ [22, 23]. Second, the polarization $P^{\rm BTO}$, is obtained for each sample from the TO_4 optical-phonon intensity, which is proportional to P^2 [21, 28]. Third, the STO susceptibility $\chi_{\rm STO}$ is taken to be the same for all samples and to follow a temperature dependence of the kind of that given by Ref. [29] (i.e., increasing with decreasing temperature, and saturating when $T \rightarrow 0$). And finally, with all these temperature dependencies set, we leave as an adjustable parameter a constant α relating the magnitude of $\pi(z)$ in the BTO and STO layers. The calculated curves are presented with continuous curves in Fig.3, clearly providing a reasonable description of the data with a minimum of assumptions and free parameters. We note that α for all curves turns out to be almost constant, varying only between 0.75 and 1.

The interpretation of the obtained phenomenological description is quite straightforward. Since $\Delta\pi = 0$ above T_C, it follows that the folded acoustic phonon intensity

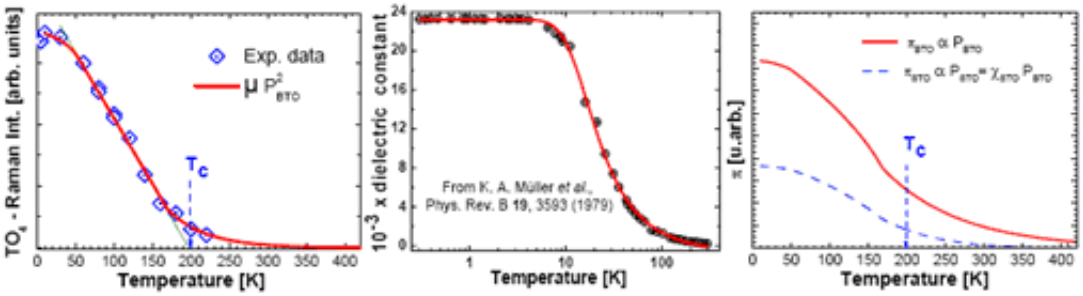

FIG. 5: Example of application of the proposed model to the analysis of the temperature dependence of the FA-phonon intensity for a BTO/STO SL with T_C of approximately 200 K. Left: derivation of the temperature dependence of the BTO polarization P^{BTO} from a fit to the T-dependence of the TO_4 optical-phonon peak intensity [16]. Center: fit to the experimental temperature dependence of bulk χ_{STO} with data from Ref.[29]. For the SLs a similar behavior was used, letting for a variation of the temperature at which χ_{STO} becomes constant in account of possible changes of this quantum behavior at nanoscale thicknesses. χ_{STO} was otherwise taken the same for all SLs with the same number of STO units cells m. Right: Temperature dependence of $\pi(z)$ taken for the BTO layers as $\pi_{BTO} \propto P^{BTO}$ and $\pi_{STO} \propto \chi_{STO} P^{BTO}$. The difference in effective photoelastic constant $\Delta\pi = \pi_{BTO} - \pi_{STO}$determines the temperature dependence of the FA-phonon Raman intensity.

originated from this mechanism should decay with increasing temperature and should disappear at the phase transition, in agreement with the data shown in Fig.3 for a series of SLs with T_C ranging from approximately 140 K to 490 K. The non observation of scattering above T_C implies, in addition, that the standard deformation potential mechanism based on $p(z)$ is comparatively negligible in the studied nanostructures and experimental conditions. When the temperature is reduced below T_C the polarization induced in the STO layers should increase because of the critical enhancement of the susceptibility χ_{STO} as $T \rightarrow 0$. This is expected to result in a *reduction* in the spatial modulation of P [17]. The consequence is a decrease in $\Delta\pi(z)$ and consequently of the Raman intensity as $T \rightarrow 0$, as in fact is observed for the SLs studied in Fig.3. The fact that the local polarization is not strongly modulated at $T = 0$ throughout thin SLs as the ones studied here, is consistent with published first-principles density-functional calculations [17]. On the other hand, our results clearly indicate that the modulation of P augments with increasing temperature, before decreasing as T approaches T_C.

The *difference* in ferroelectric polarization between the BTO and STO layers is expected to be smaller for thinner STO spacers [25, 30]. Thus, a smaller m should lead to a weaker spatial modulation $\Delta\pi(z)$ and consequently to a decrease in FA peak intensity, as experimentally verified in Fig.4. A reduction in $\Delta\pi(z)$ could also be obtained by an external polarizing field, thus opening the way to a voltage-controlled light-scattering and coherent phonon generation mechanism [31]. We note in ending that the spatial variation of $\pi(z)$ is much more rounded as compared with $p(z)$ [25, 30]. This implies that the predominant component of $\Delta\pi(z)$ should correspond to the first reciprocal lattice vector $G = 2\pi/d_{SL}$ (d_{SL} is the SL period), thus providing a possible clue to our observation of *only* the first

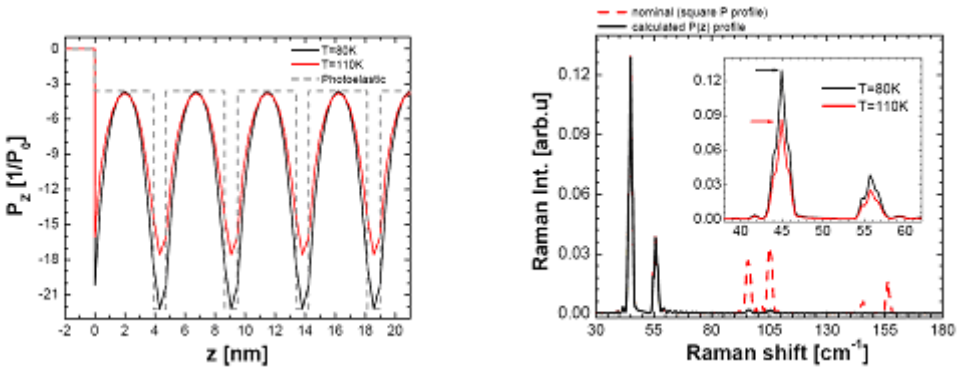

FIG. 6: Atomistic shell-model simulations of polarization profiles for two temperatures (80 K and 110 K) for a BTO_2/STO_{10} SL. The dashed lines corresponds to the square (nominal) effective photoelastic profile. (right) Calculated FA phonon Raman intensity (at T = 80 K) using the photoelastic model that accounts for the proposed ferroelectric polarization mediated scattering mechanism (full curve) and with the square-like photoelastic profile (dashed curve). Inset: comparison of the calculated Raman intensity for two different temperatures using the calculated ferroelectric polarization profiles (left panel) as input.

folded phonon doublets in all the studied oxide SLs.

To verify this hypothesis we have performed atomistic shell-model simulations of the polarization profile for a BTO_2/STO_{10} SL at two temperatures 80 K and 110 K (shown in the left panel of Fig.6). The details of the model used can be found in Ref. [32]. The calculations fix the lattice parameter to that of the substrate, STO, and allow for the formation of domains. The latter lead to the energetically most stable configuration. In addition, only when domains are allowed a significant spatial modulation of the polarization appears, which is consistent with the observed ferroelectricity induced folded-acoustic phonon Raman scattering. Note that in the calculated profiles, as already commented above, with a decrease in the temperature, the modulation of P increases, following the establishment of the ferroelectric polarization P^{BTO}. We show in Fig.6 (right), the Raman spectra calculated using Eq.1 and with these polarization profiles as input to obtain $\pi(z)$. These spectra are compared in Fig.6 with a FA-spectra calculated using the square-like photoelastic profiles standard for semiconductor SLs. It is clear that for the rounded P (and hence $\pi(z)$) profile only the first-order FA-doublet is intense, while several replicas can be clearly observed using a more square-like photoelastic $p(z)$ applicable for semiconductors, in agreement with the spectra shown in Fig.2 (right). Note also that, for the two calculated temperatures, below T_C, the intensity of the calculated spectra increase with a decrease in temperature, which is in agreement with the temperature dependencies displayed in Fig.3.

V. CONCLUSIONS

In conclusion, we have demonstrated that the nanoscale engineering of the ferroelectric polarization in $BaTiO_3/SrTiO_3$ SLs leads to a T-dependent coupling between light and THz folded acoustic vibrations. A strong dependence of the Raman intensity with the ferroelectric polarization is demonstrated, with samples that vary the ferroelectric T_C by hundreds of degrees due to the nanoscale structure of the superlattices. The results are compared with a Raman efficiency model that includes a novel ferroelectricity-induced mechanism for the scattering by folded acoustic phonons. The observed light-scattering mechanism involves the strong piezoelectricity and biased quadratic electro-optic effect existent in these oxides below T_C. Results on atomistic shell-model simulations of the ferroelectric polarization also provide clues for understanding the temperature dependence of the FA-intensity and the fact that no high-order replicas of the FA-doublets are observed. These results reflect the strong coupling between electronic, vibrational, and photonic degrees of freedom in these multifunctional nanoscale ferroelectrics. They also open interesting new perspectives in the search for multifunctional materials with enhanced light-phonon coupling, i.e., materials that can also be used for the generation of THz radiation with the added potentiality of external field tuning. The presented high-resolution UV-Raman measurements demonstrate, in addition, the power of this technique for the characterization of large gap nanoscale materials and devices.

Acknowledgments

We thank N. D. Lanzillotti-Kimura for discussions in the first stage of this investigation and G. Rozas for help in the measurement of the T-dependence of the semiconductor FA-phonon spectra displayed in Fig. 2.

References

* Electronic address: afains@cab.cnea.gov.ar

[1] C.-K. Sun, J.-C. Liang, and X.-Y. Yu, Phys. Rev. Lett. **84**, 179 (2000).
[2] Ümit Özgür, Chang-Won Lee, and Henry O. Everitt, Phys. Rev. Lett. **86**, 5604 (2001).
[3] G. D. Sanders, C. J. Stanton, and C. S. Kim, Phys. Rev. B **64**, 235316 (2001); *ibid* **66**, 079903(E) (2002); see also G.-W. Chern, K.-H. Lin, C.-K. Sun, J. Appl. Phys. **95**, 1114 (2004).
[4] B. A. Glavin *et al.*, Phys. Rev. B **71**, 081305(R) (2005).
[5] G. Rozas, M. F. Pascual Winter, A. Fainstein, B. Jusserand, P. O.Vaccaro, S. Saravanan, and N. Saito, Phys. Rev. B **72**, 035331 (2005).
[6] G. Rozas, M. F. Pascual Winter, A. Fainstein, B. Jusserand, P. O.Vaccaro, and S. Saravanan, Phys. Rev. B **77**, 165314 (2008).
[7] A. Bruchhausen *et al.*, Phys. Rev. Lett. **101**, 197402 (2008).
[8] M. R. Armstrong *et al.*, Nature Phys. **5**, 285 (2009).
[9] M. Dawber *et al.*, Rev. Mod. Phys. **77**, 1083 (2005).
[10] C. H. Ahn *et al.*, Science **303**, 488 (2004).

[11] J. Junquera and P. Ghosez, Nature **422**, 506 (2003).
[12] D. D. Fong *et al.*, Science **304**, 1650 (2004).
[13] K. J. Choi *et al.*, Science **306**, 1005 (2005).
[14] J. H. Haeni *et al.* Nature **430,** 758 (2004).
[15] S. Tinte *et al.*, Phys. Rev. B **64**, 235403 (2001).
[16] D. A. Tenne *et al.*, Science **313**, 1614 (2006).
[17] J. B. Neaton and K. M. Rabe, Appl. Phys. Lett **82**, 1586 (2003).
[18] M. Trigo *et al.*, Phys. Rev. Lett. **89**, 227402 (2002).
[19] A. Soukiassian *et al.*, Appl. Phys. Lett. **90**, 042909 (2007).
[20] V. Dvorak, Phys. Rev. **167**, 525 (1968).
[21] P. A. Fleury *et al.*, Phys. Rev. Lett. **26**, 1331 (1971).
[22] M. DiDomenico Jr. and S. H. Wemple, J. Appl. Phys. **40**, 720 (1969); S. H. Wemple *et al.*, Appl. Phys. Lett. **12**, 209 (1968).
[23] S. H. Wemple and M. DiDomenico Jr., Phys. Rev. B **1**, 193 (1970).
[24] D. G. Schlom, *et al.*, Mater. Sci. Eng. B **87**, 282 (2001).
[25] M. Sepliarsky *et al.*, Phys. Rev. Lett. **96**, 137603 (2006).
[26] K. van Benthem, C. Elsasser, and R. H. French, J. Appl. Phys. **90**, 6156 (2001).
[27] B. Jusserand and M. Cardona, in *Light Scattering in Solids V*, edited by M. Cardona and G. Guntherodt (Springer-Verlag, Berlin, 1989).
[28] K. B. Lyons *et al.*, Phys. Rev. B **17**, 2403 (1978).
[29] K. A. Muller *et al.*, Phys. Rev. B **19**, 3593 (1979).
[30] M. Sepliarsky *et al.*, Phys. Rev. B **64**, 060101 (2001).
[31] Pei-Hsun Wang *et al.*, Appl. Phys. Lett. **95**, 143108 (2009).
[32] M. Sepliarski and S. Tinte, Physica B : Condensed Matter **404**, 2730 (2009).